Acta Neuropathol
DOI 10.1007/s00401-017-1699-5

ORIGINAL PAPER

The spectrum of neuropathological changes associated with congenital Zika virus infection

Leila Chimelli[1] · Adriana S. O. Melo[2,3] · Elyzabeth Avvad-Portari[4] · Clayton A. Wiley[5] · Aline H. S. Camacho[1] · Vania S. Lopes[6] · Heloisa N. Machado[4] · Cecilia V. Andrade[4] · Dione C. A. Dock[4] · Maria Elisabeth Moreira[4] · Fernanda Tovar-Moll[7] · Patricia S. Oliveira-Szejnfeld[8] · Angela C. G. Carvalho[6] · Odile N. Ugarte[6] · Alba G. M. Batista[3] · Melania M. R. Amorim[2] · Fabiana O. Melo[2] · Thales A. Ferreira[2] · Jacqueline R. L. Marinho[3] · Girlene S. Azevedo[2] · Jeime I. B. F. Leal[3] · Rodrigo F. Madeiro da Costa[7] · Stevens Rehen[7] · Monica B. Arruda[9] · Rodrigo M. Brindeiro[9] · Rodrigo Delvechio[9] · Renato S. Aguiar[9] · Amilcar Tanuri[9]

Received: 3 December 2016 / Revised: 15 March 2017 / Accepted: 15 March 2017

Abstract A major concern associated with ZIKV infection is the increased incidence of microcephaly with frequent calcifications in infants born from infected mothers. To date, postmortem analysis of the central nervous system (CNS) in congenital infection is limited to individual reports or small series. We report a comprehensive neuropathological study in ten newborn babies infected with ZIKV during pregnancy, including the spinal cords and dorsal root ganglia (DRG), and also muscle, pituitaries, eye, systemic organs, and placentas. Using in situ hybridization (ISH) and electron microscopy, we investigated the role of direct viral infection in the pathogenesis of the lesions. Nine women had Zika symptoms between the 4th and 18th and one in the 28th gestational week. Two babies were born at 32, one at 34 and 36 weeks each and six at term. The cephalic perimeter was reduced in four, and normal or enlarged in six patients, although the brain weights were lower than expected. All had arthrogryposis, except the patient infected at 28 weeks gestation. We defined three patterns of CNS lesions, with different patterns of destructive, calcification, hypoplasia, and migration disturbances. Ventriculomegaly was severe in the first pattern due to midbrain damage with aqueduct stenosis/distortion. The second pattern had small brains and mild/moderate (ex-vacuo) ventriculomegaly. The third pattern, a well-formed brain with mild calcification, coincided with late infection. The absence of descending fibres resulted in hypoplastic basis pontis, pyramids, and cortico-spinal tracts. Spinal motor cell loss explained the intrauterine akinesia, arthrogryposis, and neurogenic muscle atrophy. DRG, dorsal nerve roots, and columns were normal. Lympho-histiocytic inflammation was mild. ISH showed meningeal, germinal matrix, and neocortical infection, consistent with neural progenitors death leading to proliferation and migration disorders. A secondary ischemic process may explain

Electronic supplementary material The online version of this article (doi:10.1007/s00401-017-1699-5) contains supplementary material, which is available to authorized users.

✉ Leila Chimelli
chimelli@hucff.ufrj.br

[1] Laboratory of Neuropathology, State Institute of Brain Paulo Niemeyer and Federal University of Rio de Janeiro (UFRJ), Rua do Resende 156, Rio de Janeiro, RJ CEP 20231-092, Brazil

[2] Research Institute Prof. Amorim Neto, Rua Duque de Caxias, 330, Prata, Campina Grande, PB CEP 58400506, Brazil

[3] Health Secretary Campina Grande, Rua Duque de Caxias, 330, Prata, Campina Grande, PB CEP 58400506, Brazil

[4] Fernandes Figueira Institute-FioCruz, Avenida Rui Barbosa, 716, Flamengo, Rio De Janeiro, RJ CEP 22250-020, Brazil

[5] Division of Neuropathology, UPMC Presbiterian Hospital, S701 Scaife Hall 200 Lothrop Street, Pittsburgh, PA 15213, USA

[6] Department of Pathology, Antonio Pedro University Hospital, Fluminense Federal University, Rua Marques de Paraná, 303, Centro, Niterói, RJ CEP 24033-900, Brazil

[7] D'Or Institute for Research and Education (IDOR) and UFRJ, Rua Diniz Cordeiro, 30, Botafogo, Rio De Janeiro, RJ CEP 22281-100, Brazil

[8] Fetal Medicine Research, Foundation Institute for Education and Research in Diagnostic Imaging (FIDI), Rua Napoleão de Barros, 800, Vila Clementino, São Paulo, SP CEP 04024-002, Brazil

[9] Laboratory of Medical Virology, Departamento de Genética, Instituto de Biologia, CCS, Bloco A, sala 121, UFRJ, Rio De Janeiro, RJ CEP 21941-902, Brazil

Published online: 22 March 2017

the destructive lesions. In conclusion, we characterized the destructive and malformative consequences of ZIKV in the nervous system, as reflected in the topography and severity of lesions, anatomic localization of the virus, and timing of infection during gestation. Our findings indicate a developmental vulnerability of the immature CNS, and shed light on possible mechanisms of brain injury of this newly recognized public health threat.

Keywords Zika virus · Congenital ZIKV infection · Microcephaly · Calcification · In situ hybridization · Neuropathology

Introduction

A widespread epidemic of Zika virus (ZIKV) infection was reported in 2015 in South and Central America [10, 21, 35]. Symptoms varied from mild fever, arthralgia, rash, headache, and myalgia, but frequently infection was asymptomatic [2, 5]. More severe sequelae of ZIKV infection in adults included Guillain–Barré syndrome, acute myelitis, and meningoencephalitis [2, 8, 30]. A major concern associated with ZIKV infection was the increased incidence of microcephaly in infants born from infected mothers [20, 22, 37]. In addition, other malformations including ventriculomegaly, cerebellar hypoplasia, and fetal akinesia deformation sequence (arthrogryposis) were associated with congenital Zika infection [5, 31, 41]. Calcification, detected with cerebral ultrasound, was an early hallmark [32, 34].

ZIKV, an arbovirus of the *Flaviviridae* family, genus *Flavivirus*, was initially isolated in 1947 from serum of a sentinel rhesus macaque in the Zika forest, Uganda [13]. Subsequent isolations of the virus were obtained from mosquitoes of genus *Aedes*, implicating these insects as vectors [21]. Since then, occasional human cases occurred in Africa and Asia. In 2007, a large outbreak was registered on Yap Island in Micronesia, caused by the Asian ZIKV lineage [15]. During 2013 and 2014, many outbreaks occurred in French Polynesia [4]. The virus arrived in Brazil, where in 2015, autochthonous transmission was reported for the first time in Bahia and Rio Grande do Norte [7, 49]. In less than 1 year, ZIKV spread to many Brazilian states (particularly in the Northeast) and is currently endemic in many Latin America countries and the Caribbean [10, 21]. Recently, a series of autochthonous cases have been reported in Miami, USA [26]. The ability to infect widely distributed species of Aedes mosquitoes led to its rapid dissemination and made ZIKV an enormous threat to other countries [28, 39].

In the beginning of 2016, the first autopsied case of microcephaly associated with ZIKV was reported after interruption of pregnancy at 32 weeks of gestation [32]. Besides microcephaly, there were almost complete agyria and multifocal dystrophic calcifications in the cortex and subcortical white matter. This case was followed by several other reports showing similar lesions including microglial nodules, gliosis, nerve cell degeneration, and necrosis [12, 14, 29, 36]. In all cases, the authors reported the detection of ZIKV in fetal and newborn brain tissue, either by reverse transcriptase–polymerase-chain-reaction assay, electron microscopy and/or immunohistochemistry, in one of them from extracts of CNS, since autopsy was not allowed [36].

To date, neuropathological descriptions of congenital Zika viral infection have been limited to individual case reports or very small series and a more comprehensive CNS analysis in series of cases is needed [28, 38, 42]. Herein, we report the neuropathological findings associated with congenital ZIKV infection in ten stillborn or newborn babies who died within the first 37 h of life. Using postmortem tissue and in situ hybridization, we investigated the role of direct viral infection in the pathogenesis of Zika-associated lesions and malformations.

Materials and methods

Patients

The CNS of ten stillborn or newborn babies who died in the first 37 h of life, three (cases #3, 6, 9) from northeastern state of Paraiba (PB) and seven (cases #1, 2, 4, 5, 7, 8, 10) from the southeastern state of Rio de Janeiro (RJ), Brazil, whose mothers reported typical symptoms of ZIKV infection between the 4th and the 28th gestational weeks, were examined postmortem. They were identified according to time of maternal symptoms. The cases from RJ were part of the normal autopsy catchment of the pathology departments involved. The autopsies in babies from PB were performed in the hospital where they were born and formalin-fixed tissue was shipped to Rio de Janeiro. This study was approved by the local internal review board (IRB) under the number 52888616.4.0000.5693. Informed consent was obtained from all parents of participants included in the study.

Neuroimaging studies

Intrauterine fetal development was followed with ultrasonography and fetal MRI. Just after birth, the cephalic perimeter was measured and the percentile was calculated according to the expected for the gestational age [40]. In the three neonates from the state of PB, postmortem formalin-fixed brain tissue imaging was acquired on a 64-channel multislice computed tomography (CT) (GE Healthcare) and 3T MRI scanner (Achieva, Phillips, The Netherlands) and correlated with the neuropathological findings. One of them (#6) was also submitted to a postmortem CT before the autopsy.

Zika virus diagnostic procedures

ZIKV RNA was investigated in the mothers or babies through RT-PCR targeting the *env* gene as described elsewhere [24]. ZIKV was detected in fluid samples including blood, urine, amniotic fluid obtained by amniocentesis during gestation, or in other fluids after birth (amniotic fluid and/or blood cord). In the three neonates from the state of PB, postnatal ZIKV infection investigations were also performed in the autopsy tissues (placenta or brain and other organs). Viral RNA was extracted from 140 µl fluids using QIAmp MiniElute Virus Spin (QIAgen, Hilden, Germany), following the manufacturer's recommendations. ZIKV detection was performed using One Step Taqman RT-qPCR (Thermo Fisher Scientific, Waltham, MA, United States) on 7500 Real-time PCR System (Applied Biosystems, Foster City, CA, United States) with primers, probes, and conditions as described elsewhere [24]. Fifty milligrams of frozen organs such as cerebral cortex, heart, skin, spleen, thymus, liver, kidneys, lung, and placenta were disrupted using Tissuerupter® (QIAgen, Hilden, Germany) using 325 µl of RTL buffer from RNEasy Plus mini Kit (QIAgen, Hilden, Germany), following the manufacturer's protocol. RNA was extracted with the use of a TRIzol Plus RNA purification kit (Thermo Fisher Scientific, Waltham, MA, United States). Real-time RT-PCR for the detection of ZIKV RNA targeting the envelope gene was performed using 1 µg of total tissue RNA using The Applied Biosystems® TaqMan® RNA-to-C_T™ 1-Step Kit as described above.

Dengue and Chikungunya virus infections were excluded by ELISA and PCR in all cases. TORCHS (Toxoplasmosis, Rubella, Cytomegalovirus, Herpes virus, and Syphilis), HIV, and parvovirus B19 antibody titers were negative.

Autopsies

Full autopsies were performed and the brains were fixed in 10% buffered formalin. In the three cases from the state of PB, one hemisphere was stored in RNA later and then frozen for virological and molecular analysis. In seven cases, the whole spinal cords were also removed, four of them with DRG. The upper cervical spinal cord was also sampled in two other cases, one with DRG. Formalin-fixed brains were weighed and the percentile was calculated according to the expected for the gestational age [25].

In addition, samples from skeletal muscle (paravertebral, psoas, diaphragm or adjacent to head of femur) were taken and examined histologically in five cases, the pituitary in two cases and one eye in one case. Some CNS lesions of two of these patients (#3 and 9) have been reported previously [31] as part of a multidisciplinary approach for congenital Zika infection, but the complete spectrum of neuropathological findings was not fully available at that time.

After gross examination, representative areas, including those with macroscopic lesions, were processed for paraffin embedding and 5 µm histological sections were stained with hematoxylin and eosin (H&E). From selected blocks of the cerebral hemispheres, brainstem, cerebellum, and spinal cord, 10 µm sections were stained with Luxol Fast Blue (LFB) for myelin.

Placentas

A detailed macroscopic and microscopic analysis of five placentas and umbilical cords from the state of RJ (patients #2, 5, 7, 8, 10) and the microscopic analysis of fragments of the three placentas and umbilical cords from the state of PB (patients #3, 6, 9) are included in this study.

Immunohistochemistry

From the leptomeninges, choroid plexus and selected areas of the nervous tissue which presented histological lesions, immuno-histochemical reactions were performed, using the following monoclonal antibodies (Cell Marque, Sigma-Aldrich Co, Rocklin, CA, USA) and dilutions: anti-glial fibrillary acidic protein- GFAP- clone EP672y, (1:500), anti-neurofilament clone 2F11 (1:2000), anti-CD3 clone MRQ39 (1:1000), anti-CD20 clone SP32 (1:1000), anti-CD8 clone C8/144B (1:1000), anti-CD68 clone Kp-1 (1:1000), anti-Olig2 clone 211F1.1 (1:200), and anti-NeuN (Zeta Corporation, Arcadia, CA, USA) Clone A100 (1:200). Five µm-thick tissue sections were incubated in a drying oven at 37 °C for 6 h and then deparaffinized in xylene. The tissue sections were rehydrated by placing in decreasing concentrations of alcohol and washed in distilled water. To enhance antigen retrieval, the tissue sections were pretreated in an Electric Pressure cooker for 15 min in the solution 1:20 Declere® (pH 6)/1:100 Trilogy (pH 9) in distilled water. To block endogenous peroxidase activity, the tissue sections were exposed to hydrogen peroxide, washed with distilled water, and rinsed in phosphate buffered saline (PBS) to stop enzymatic digestion. They were then incubated with the primary antibody overnight at 4 °C, rinsed in PBS for 5 min, and incubated with Polymer Hi Def (horseradish peroxidase system) for 10 min at room temperature preceded by several washes in PBS. The peroxidase reaction was visualized with DAB substrate and rinsed in running water; the sections were then counterstained with Meyer's hematoxylin for 1 min, washed in running tap water for 3 min, dehydrated in alcohol, cleared in xylene, and mounted in resinous medium. Technical details are found in http://www.cellmarque.com/cms/about.php and http://www.zeta-corp.com.

Transmission electron microscopy

Areas of interest from two formalin-fixed brain fragments (cases #5 and 9) were carefully selected and immersed in 2.5% glutaraldehyde (v/v), 0.1 M Na-cacodylate buffer (pH 7.2), postfixed in 1% OsO4 in cacodylate buffer with 5 mM calcium chloride and 0.8% potassium ferricyanide. Brain fragments were then washed in PBS, dehydrated in increasing acetone concentrations, and embedded in EPON. Ultrathin sections (70 nm) were collected on 300 mesh copper grids, stained with uranyl acetate and lead citrate, and observed at 80 kV with a Zeiss 900 (Carl-Zeiss, Jena, Germany) transmission electron microscope.

ZIKV in situ hybridization

ISH studies were performed on formalin-fixed paraffin embedded (FFPE) tissue sections of all brains, placenta (7 cases), liver (8 cases), kidney (8 cases), spleen (7 cases), intestine (6 cases), heart (6 cases), adrenal (4 cases), and thymus (2 cases), using two commercial RNAscope Target Probes (Advanced Cell Diagnostics, Hayward, CA, United States) catalog #464531 and 463781 complementary to sequences 866-1763 and 1550-2456 of ZIKV genome, respectively. Pretreatment, hybridization, and detection techniques were performed according to the manufacturer's protocols. In the absence of control specimens of ZIKV infected cells/tissues, FFPE brain tissue section from mice infected with West Nile Virus (WNV) was used as positive controls [6]. The target probe 463781 detected WNV infected brain tissue, while the 464531 probe did not (data not shown). Both probes detected Zika virus in the test specimens.

Results

A summary of the results is presented in Table 1.

Clinical and laboratory findings

Maternal ages ranged from 18 to 37 years. All pregnant women had history of skin rash, itching, or other Zika symptoms, nine within the first 4 months of pregnancy and one in the 28th week of gestation (case #10). The babies were all born at term except four of them who were born prematurely (one at 36, one at 34 and two babies at 32 weeks). ZIKV RNA was detected in the mother blood (case #2) and urine (case #10), amniotic fluid (cases #3, 6, 9), cord blood (cases #3, 9), and samples of postmortem neonatal organs and brain (cases #3, 6, 9). The ZIKV RNA load in amniotic fluid and tissues, including the brain, was higher in case #9, where the RT-PCR amplified in Ct 22.

External findings, general autopsy, and placental findings

All neonates except one (case #10) had arthrogryposis involving upper and lower limbs, although in case #2, the upper limbs only were affected. The cephalic perimeter was either reduced, normal, or enlarged, which was related to the severity of ventriculomegaly, except case #10 whose ventricles were not dilated. Microphthalmia was present in some cases. Figure 1 illustrates some of these neonates and the corresponding macroscopic appearance of their brains (described below).

In the systemic organs, there was occasional occurrence of mild viral hepatitis, and in one case (#10), pulmonary hypoplasia possibly related to adramnia. This was the cause of death in this case, while in all others, the death was due the severity of the CNS lesions, particularly in the brainstem. However, case #5, a stillborn with evidence of maternal hypertension and severe circulatory placental changes, also had myocardial infarct.

Morphological findings in the placentas included multifocal chronic villitis, stromal fibrosis with concentric hyperplasia of the muscle wall in villous vessels, stromal calcification, and focal chorionic vasculitis. Chronic focal chorionitis and deciduitis were also seen. There were also circulatory changes, such as chorangiosis, fewer vasculo-syncytial membranes, and villous dismaturity, which were more prominent in case #5, where infarcts and decidual vasculopathy (fibrinoid necrosis, thrombosis, acute atherosis, and muscular hypertrophy) were related to maternal hypertension. Most placentas were small for the gestational age. Detailed macroscopic and microscopic descriptions of each case appear in Suppl. Table 1 and Descriptions. Illustrations of some placentas are found in Suppl. 1.

ISH results for ZIKV in all placentas examined were negative, and among the systemic organs, the virus was frequently present in the liver (hepatocytes), kidney (mostly collecting tubules), and spleen (red pulp), illustrated in Suppl. 2. Systemic infection was also observed in heart (1 of 6) and 2 of 4 adrenal glands (medulla).

Imaging/pathologic correlation in the brain

Prenatal ultrasound and MRI examinations showed signs of decreased cerebral maturation and disturbance of fetal brain growth already in the first trimester of gestation, including cortical abnormalities, hypodevelopment of sulci, some of them with agyria, reduced parenchymal volume, ventriculomegaly (usually asymmetric), callosal dysgenesis, thalamic and ponto-cerebellar hypoplasia and enlarged cisterna magna, very hypodeveloped cerebellar vermis, and marked thin (nonsegmented) brainstem (Fig. 2a–neonate #3). The

Table 1 Identification of neonates, ordered by gestational week of maternal symptoms; diagnosis of ZikV infection; main groups of lesions

Patient, sex, age	1, F, 37 h	2, M, 29 h	3, F, 20 h	4, M, 24 min	5, F, stillborn	6, M, 15 min	7, M, stillborn	8, F, 12 h	9, M, 10 h	10, M, stillborn
Gestational week of Zika symptoms	4.5	5.5	8	9	10	12	16	16	18	28
Gestational week at birth	32	38	36	40 and 6 days	32	41	41	40	41	34 and 5 days
Zika PCR results	not available	Mother blood	Amniotic fluid, cord blood, brain	Not available	Not available	Amniotic fluid, brain	Not available	Negative	Amniotic fluid, cord blood, brain	Urine
Zika ISH–CNS	Negative	Meninges	Meninges	Meninges	Meninges, neocortex, germinal matrix	Negative	Negative	Negative	Meninges	Negative
Zika ISH in other organs	Liver, kidney adrenal, spleen	Not available	Liver, kidney adrenal	Not available	Liver	Liver, spleen	Liver, heart	Liver	Kidney	Not available
Cephalic perimeter/ percentile	36.5 cm/>P95	36 cm/P95	35,0 cm/P95	26 cm/<P3	21 cm/<P3	29.5 cm/<P3	37.5 cm/>P95	26 cm/<P3	36.5 cm/P95	29/P5
Brain weight/ percentile	48 g/< P10	50 g/< P10	232 g/P10	32 g/< P10	7 g/<P10	90 g/< P10	180 g/<P10	49 g/<P10	78 g/<P10	280 g/P75
Ventriculo-megaly	+++	+++	+++	+ (Ex-vacuo)	++ (Ex-vacuo)	++ (Ex-vacuo)	+++	+ (Ex-vacuo)	+++	No
Lymphocytes and histiocytes	Meninges	No	Meninges, deep gray nuclei, brainstem	No	No	Meninges, deep gray nuclei,	Meninges, brainstem	Meninges	Deep gray nuclei, brainstem	Choroid plexus
Destructive lesions/ calcification	+++ Hemi-spheres, deep gray nuclei, brainstem + spinal anterior horn	+++ Hemi-spheres, deep gray nuclei, brainstem, spinal anterior horn	+++ Deep gray nuclei, brainstem	+++ Hemi-spheres, deep gray nuclei, spinal anterior horn	+++ Hemi-spheres; + spinal anterior horn, cerebellar necrosis	+++ Hemi-spheres, deep gray nuclei; + brainstem, spinal anterior horn	+++ Deep gray nuclei, brain-stem; + spinal anterior horn	+++ Hemi-spheres, deep gray nuclei; + spinal anterior horn	+++ Brain-stem	+ Hemispheres
Migration disturbances	MGNH; AICC	MGNH; AICC; CCDH	PMG; AICC; CCD	MGNH; PMG; AICC; CCD	PMG; AICC	MGNH; AICC; PMG; CCDH	MGNH; AICC; PMG; CCDH	MGNH; PMG; AICC; CCDH	MGNH; PMG	AICC
Hypoplasia[a] of CNS structures[b]	Yes	Yes	Yes	Yes	Yes	Yes	Yes	Yes	Yes	No
Spinal anterior horn cell loss	Yes	Yes, sparing lumbar level	Yes (sampled cervical only)	Yes	Yes	Yes (sampled cervical only)	Yes	Yes	Spinal cord not sampled	No

Table 1 continued

Patient, sex, age	1, F, 37 h	2, M, 29 h	3, F, 20 h	4, M, 24 min	5, F, stillborn	6, M, 15 min	7, M, stillborn	8, F, 12 h	9, M, 10 h	10, M, stillborn
Neurogenic muscle atrophy	Muscle not sampled	Upper limbs only	Yes	Muscle not sampled	Yes	Muscle not sampled	Yes	Yes	Muscle not sampled	Muscle not sampled
Arthrogryposis	Yes	Upper limbs	Yes	Yes	Yes	Yes	Yes	Yes	Yes	No

Mild (+); Moderate (++); Severe (+++)

H hours, *mins* minutes, *F* female; *M* male

MGNH meningeal glioneuronal heterotopia, *PMG* polymicrogyria, *CCD* cerebellar cortical dysplasia, *CCDH* cerebellar cortical dysplasia & heterotopia, *AICC* abnormal immature cell clusters

[a] Here as consequence of destruction of sites leading to subsequent atrophy or hypotrophy

[b] Deep gray nuclei, corpus callosum, cerebellum, brainstem, descending motor fibres (small basis pons, pyramids, and lateral cortico-spinal tracts)

corresponding cerebral hemisphere is illustrated in Fig. 2b. Intracranial calcifications were common, particularly in the gray–white matter junction, the basal ganglia and/or thalamus, and the brainstem. The skull frequently had a collapsed appearance with overlapping sutures.

Postmortem brain CT scan of the neonate #6 (Fig. 2c), in addition to a smooth surface, ventriculomegaly particularly in the occipital region (colpocephaly), showed calcification in various regions, including the gray–white matter junction, basal ganglia, and thalami. The macroscopic appearance of the formalin-fixed cerebral hemisphere is illustrated in Fig. 2d.

MRI of formalin-fixed brain tissue, performed in cases #3, 6, and 9, confirmed the cortical abnormalities, under development of sulci, agyria, reduced parenchymal volume, and ventriculomegaly. In addition, formalin-fixed brain CT scan of case #3 showed calcification in the hypothalamic/brainstem transition, confirmed macro and microscopically. The neuroimaging appearances of cases #3, 6, and 9, from the state of PB, were reported elsewhere [41].

Macroscopic findings in the brain and spinal cord

Cerebral hemispheres and ventricles

Leptomeninges were focally thickened (Fig. 2b), and there was ventriculomegaly, frequently asymmetric, particularly in the occipital lobes (Fig. 2d), where the parenchyma was very thin (Fig. 1h). In these cases, the amount of cerebrospinal fluid (CSF) could reach 400 ml (Suppl. 3a), as in case #1, and the brain usually collapsed after removal of the skull (Fig. 1f; Suppl. 4a). On the other hand, when the brains were too small (Fig. 1e, g), the cranial bones were overlapped or fused (Suppl. 4b) and there was mild-to-moderate ventriculomegaly (ex-vacuo). Shallow sulci or agyria was frequent (Fig. 2b, d; Suppl. 6) and a cobblestone appearance could be observed in agyric areas (Fig. 3a). The hippocampus was usually not well identified, in one case, it was vertically oriented and in the other, malformed. The corpus callosum was either absent or very thin. In regions where the cerebral hemispheres were slightly thicker, the white matter was translucent, as in case #3, infected early in gestation, which was less evident in case #10, infected at the 28th week (Suppl. 5).

Basal ganglia and thalami were small, usually malformed or not well recognized (Fig. 1h; Suppl. 6b).

Posterior fossa structures were markedly reduced in size. There was cerebellar hypoplasia with irregular or smooth cortical surface and the 4th ventricle was enlarged (Fig. 4a, b). One cerebellar hemisphere of the smallest brain was brownish and liquefied (Fig. 1e). The brainstems were frequently small, particularly the basis

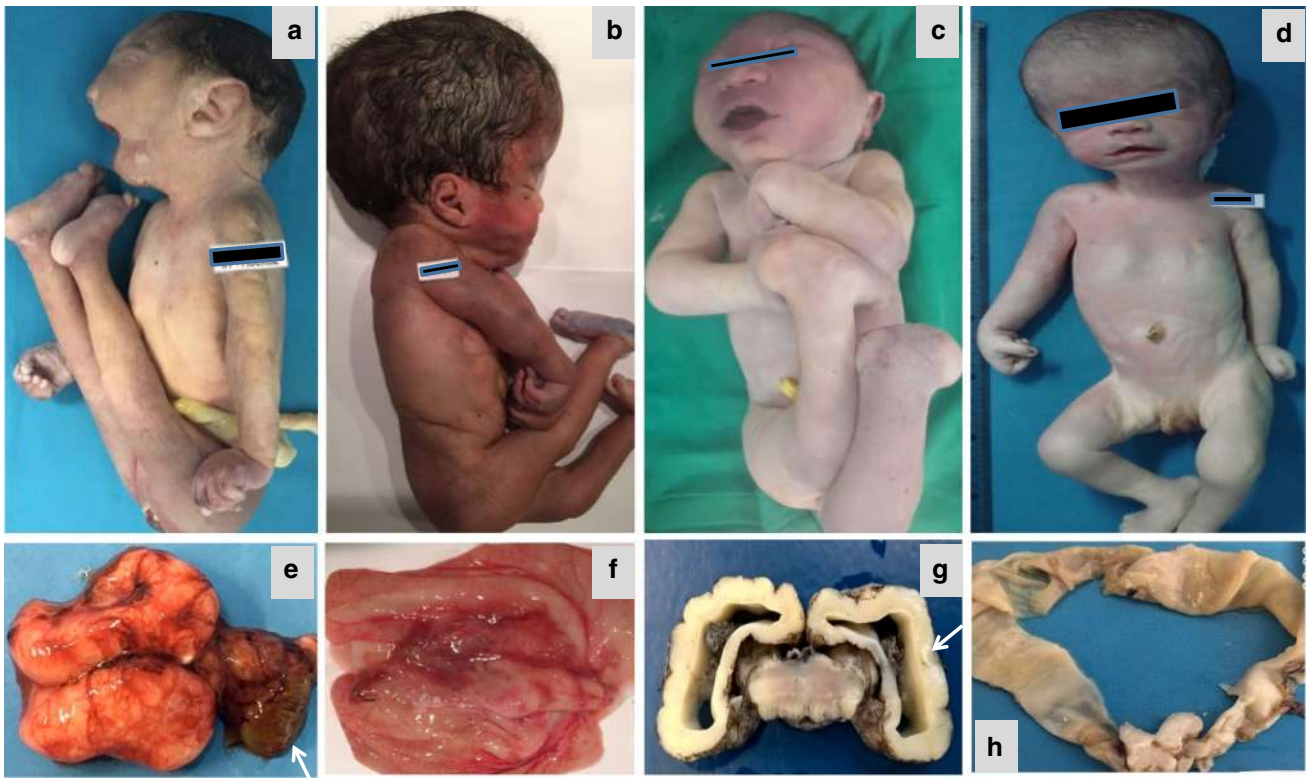

Fig. 1 Some of the neonates included in this series. **a**, **b**, **c** (Cases #5, 1, 4) with arthrogryposis in all four limbs. **d** (case #2) with arthrogryposis in upper limbs only. Microcephaly is observed in **a** and **c**. Enlarged cephalic perimeter due to hydrocephalus in **b** and **d**. The corresponding macroscopic appearances of their brains are shown in **e**, **f**, **g**, and **h**. The convexity of a very small brain with almost smooth surface (**e**) and ex-vacuo ventriculomegaly (**g**) is observed in those with microcephaly. Hemispheric calcification is also seen in **g** (*arrow*). The convexity of a collapsed severely hydrocephalic brain is seen in **f**, and coronal section in **h** shows very thin hemispheric parenchyma, while at the base, small malformed deep gray nuclei are present. In **e**, a *red-brownish* soft cerebellar hemisphere (*arrow*), which on section was liquefied

pontis, which in some cases was practically absent, as were the pyramids (Fig. 4e).

Calcification was detected macroscopically in the cortical mantle, junction between gray and white matter, deep gray nuclei, and brainstem (Figs. 1g, 4g; Suppl. 6). The latter was particularly prominent in cases with severe ventriculomegaly, when the midbrain was distorted and the aqueduct was not visible (Fig. 4g). When the brains were very small (Fig. 1e, g; Suppl. 4b), with ex-vacuo ventriculomegaly, the aqueduct was patent, even dilated (Fig. 4d), as was the 4th ventricle, but coarse calcification was not detected in the brainstem.

The spinal cord was usually thin and DRG could be identified (Fig. 4h). Hypoplasia of the optic chiasm and nerves were also present in some cases. In only one case (#10), the CNS was well developed and the only macroscopic change was calcification in deep hemispheric white matter (Suppl. 5d).

Histopathological findings in CNS, skeletal muscle, pituitary, and eye

Cerebral cortex and leptomeninges

In cases with severe ventriculomegaly, the cerebral parenchyma was very thin, sometimes consisting of remnants of germinal matrix and leptomeninges only (Fig. 3d), where macrophages containing hemosiderin could occasionally be seen. Immunostaining for NeuN was negative in these cases (Fig. 3e), while in others, even with a slightly wider cortical mantle, nerve cells could be detected (Fig. 3f).

There were disturbances of neuronal migration in cerebral and cerebellar hemispheres and in the brainstem, including polymicrogyria (Fig. 3c), meningeal glioneuronal heterotopia (Fig. 3b), and cerebellar cortical dysplasia (Fig. 4c). Abnormally large irregular clusters of

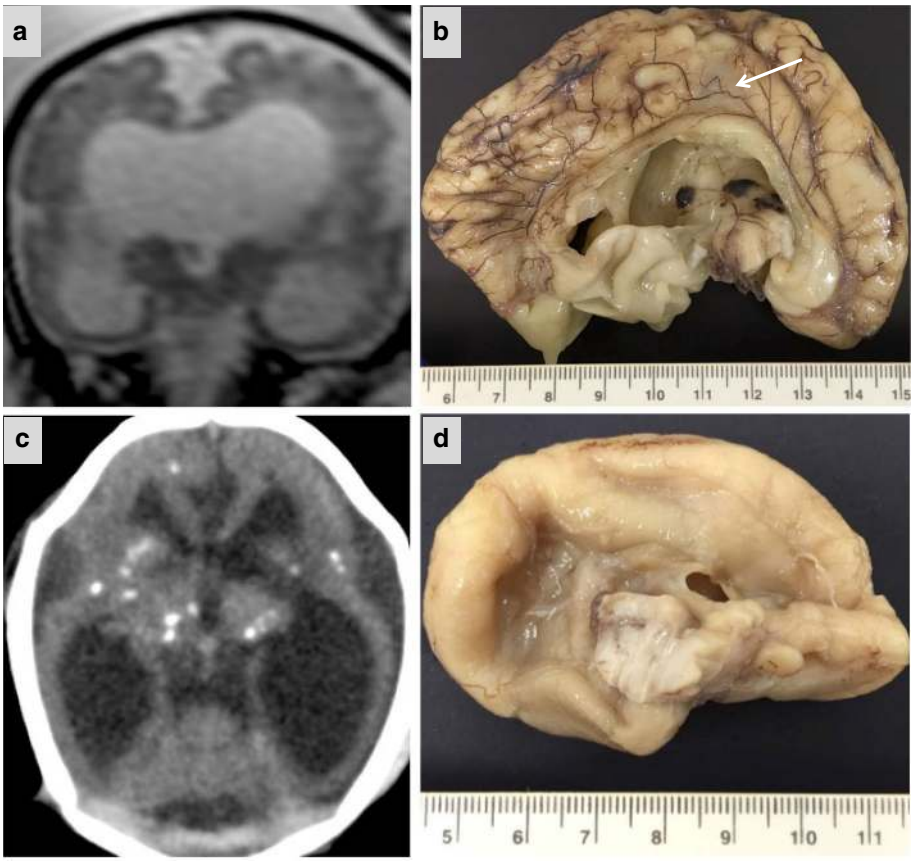

Fig. 2 **a**, **b** Case #3—**a** fetal MRI in the coronal plane at 36th weeks of gestation showing reduced brain volume, diffuse gyri abnormalities, severe ventriculomegaly, under developed cerebellar vermis and marked thin (nonsegmented) brainstem. **b** Medial view of one cerebral hemisphere with thickened (*arrow*) congested leptomeninges and shallow sulci. **c**, **d** Case #6—axial postmortem brain CT image showing decreased parenchymal volume, cortical hypo development, predominant occipital ventriculomegaly and calcifications in the *gray–white* matter junction, basal ganglia, and thalami (**c**). Medial surface of the cerebral hemisphere with smooth surface and collapsed occipital lobe due to increased ventricle (**d**)

immature cells (for the gestational age) were usually seen along the ventricular surface and towards the cortex, sometimes intermingled with fine or coarse calcification in various levels of the hemispheric parenchyma.

The ependyma showed multifocal erosions, granulations, and occasional subependymal rosettes. There was evidence of previous subependymal hemorrhage in case #5, with the presence of hemosiderin-laden histiocytes. Apoptotic bodies were occasionally observed along the ependymal surface and in some remnants of the germinal matrix. The latter had various thicknesses and were usually disorganized, depleted of cells, or intermingled with histiocytes (Suppl. 7).

In LFB stained sections, myelination, as expected, was practically absent in hemispheric white matter. However, oligodendrocytes stained with Olig 2 were not even present, except in the hemisphere of patient infected in the last trimester (case #10), where various oligodendrocytes could be detected (Suppl. 5).

In deep gray nuclei and posterior fossa structures, very few myelinated fibers were detected in the deformed internal capsule and cerebellum, while in the brainstem and spinal cord, they were evident, although distorted in the brainstem. Axons, immunostained with neurofilament, were directionally disrupted. There were also Wallerian degeneration and axonal spheroids, particularly in deep gray nuclei and the brainstem (Fig. 5d), in addition to coarse and filamentous calcification and extensive gliosis (Fig. 5c). These remarkable abnormalities of the brainstem (particularly at the level of the midbrain-Fig. 5a) were associated with aqueduct stenosis, characterized by small and displaced branching channels (Fig. 5b), and largely dilated ventricles, as shown in Fig. 1h. The basis pontis and pyramids as observed macroscopically were often small. In addition to cortical dysplasia (Fig. 4c), there was mature or immature neuronal heterotopia in the cerebellum where the dentate nuclei were usually not well recognized or represented by separate blocks of nerve cells. In case #5, the liquefied cerebellar hemisphere consisted of lipid-laden macrophages, hemosiderin, and some remaining vessels.

The spinal cords were usually abnormally shaped due to the lack, or very small cortico-spinal tracts (Fig. 6a, b, f), in addition to motor nerve cell degeneration and loss, gliosis, small, or coarse foci of calcification (Figs. 6e). Ventral roots were abnormally thinner than the dorsal ones (Fig. 6f). In one case with arthrogryposis involving mainly the upper limbs, the motor nerve cells in lumbar region were less affected. There were two central canals in at least two cases. The dorsal column was preserved and myelinated, as were the dorsal nerve roots, and the DRG. The spinal cord of case #10 was normal (Fig. 6c, d), as were the brain, cerebellum, and brainstem, except for focal hemispheric

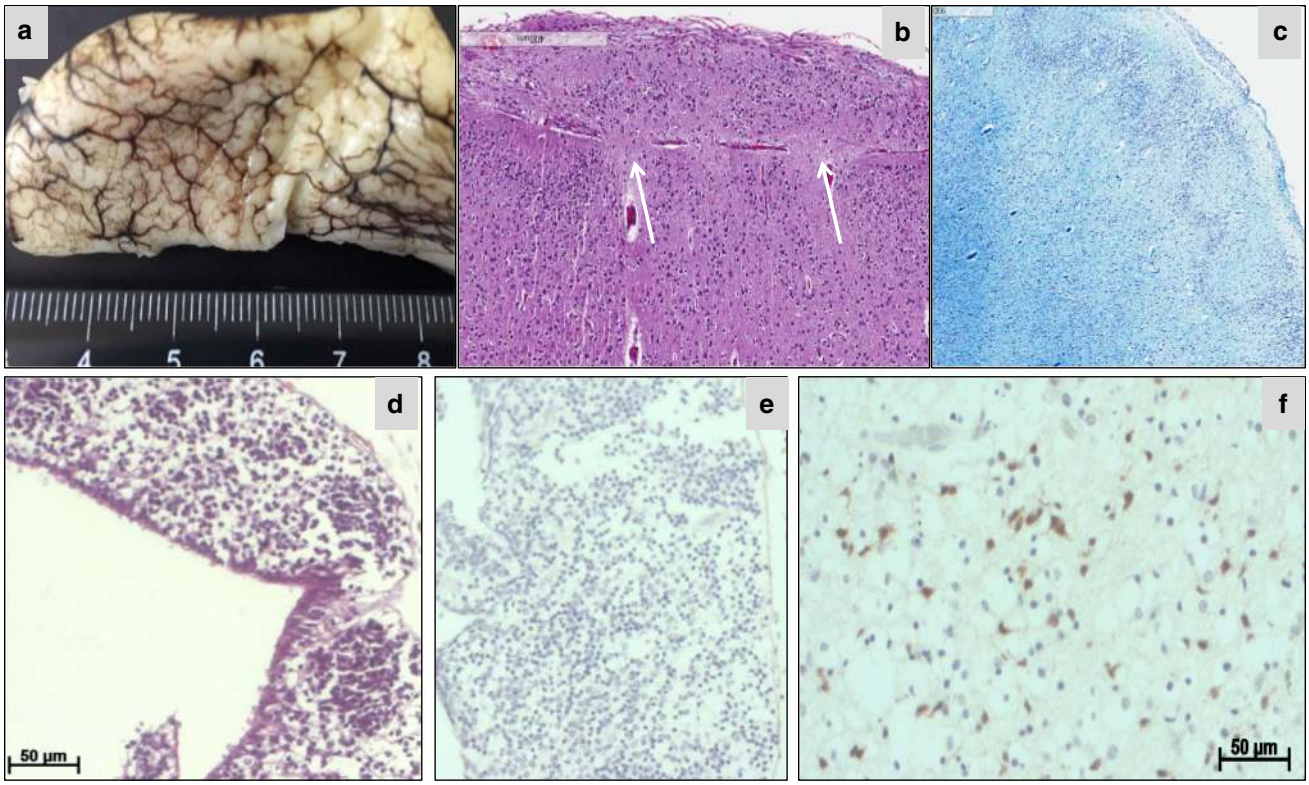

Fig. 3 **a**, **b** Case #9—**a** Segment of the agyric hemisphere shows an irregular surface with cobblestone appearance. **b** meningeal glioneuronal heterotopia. The piamater is interrupted in some regions (*arrows*), with over-migration of the cerebral tissue to the subarachnoid space (upper part of the picture). **c** Case #6—cerebral cortex with polymicrogyria. **d**, **e** Case #1—very thin cerebral parenchyma, consisting here of remnants of germinal matrix and leptomeninges only. Ependymal surface is on the left and lower part of the section. **e** Immunostaining for NeuN is negative, while in **f** (case #5), some nerve cells are immunostained. H&E (**b**, **d**), LFB (**c**); NeuN (**e**, **f**)

calcification, gliosis, and some clusters of immature cells in deep hemispheric white matter.

Inflammation was not a prominent feature in any segment of the CNS of these cases. There was mild-to-moderate lymphocytic meningitis and scattered perivascular parenchymal CD8+ T-lymphocytes, CD68+ histiocytes, microglial hyperplasia, and gliosis, but microglial nodule (Fig. 7; Suppl. 7) was seen in only one occasion (case #9). Mild lymphocytic infiltration was present in the choroid plexus of only one case (#10). No cytoplasmic or nuclear inclusions or parasites were seen.

Zika ISH in the CNS showed that the meninges were frequently infected (cases #2, 3, 4, 5, 9), but the brain parenchyma was negative, except in case #5, which was positive in the germinal matrix and the neocortex. These results are illustrated in Fig. 8.

Transmission electron microscopy of cerebral cortical surface in close contact with leptomeninges in case #9, and of the germinal matrix in case #5, despite fixation artifacts, showed vesicles containing many viral particles (Fig. 9), corroborating the detection of ZIKV with ISH.

All muscles sampled, except from the lower limb of case #2, showed neurogenic muscle atrophy (Fig. 6g). Focal microscopic calcification was observed in the two pituitaries examined (cases #7, 8) and in the retina and lens of case #5, illustrated in Suppl. 8

Discussion

Diagnosis of ZIKV infection

In this series, ZIKV infection was confirmed either using RT-PCR or ISH. Although in the beginning of our study, we tried immunohistochemistry to identify the virus in the brain tissue, as in the previous studies [12, 29], this method was abandoned because of unreliable results, with cross reactions with normal nerve cells. On the other hand, although limited to few samples, the electron microscopy of formalin-fixed tissue disclosed viral particles and could be used to confirm the presence of virus in postmortem tissue. ISH disclosed viral RNA in meninges

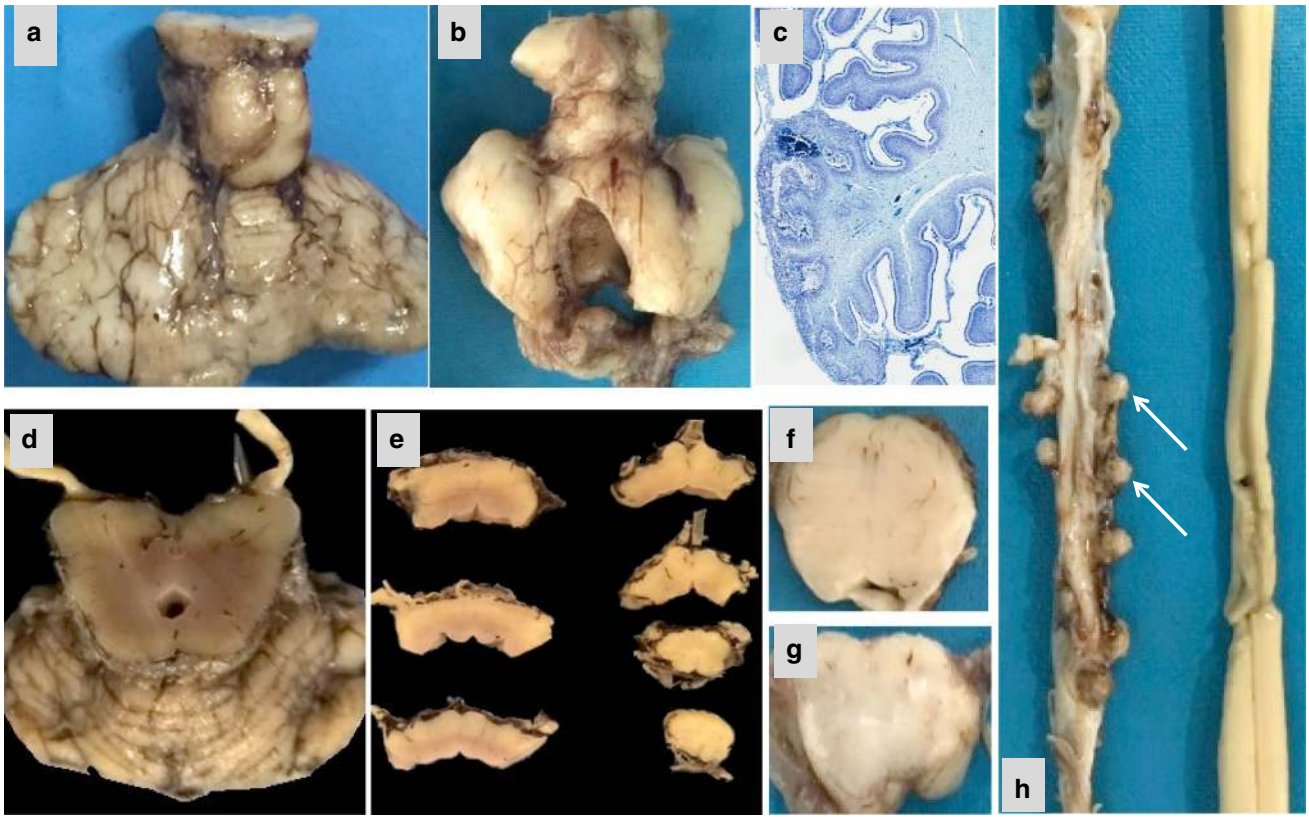

Fig. 4 Irregular or smooth cortical surface of the cerebellum of cases #7 and 2 (**a**, **b**). Markedly reduced volume of the cerebellum with corresponding enlargement of the 4th ventricle is observed in **b**. In **c** (case #3), cerebellar cortical dysplasia and no myelin in the white matter. **d**, **e** Case #4—small cerebellum, dilated aqueduct (**d**), flat basis pons, small pyramids (**e**). For comparison, the normal pons of case #10 is illustrated in **f**. **g** Case #7—distorted midbrain with *whitish* areas of calcification. **h** (case #2): a thin spinal cord; DRG are well recognized (*arrows*). (**c**) LFB

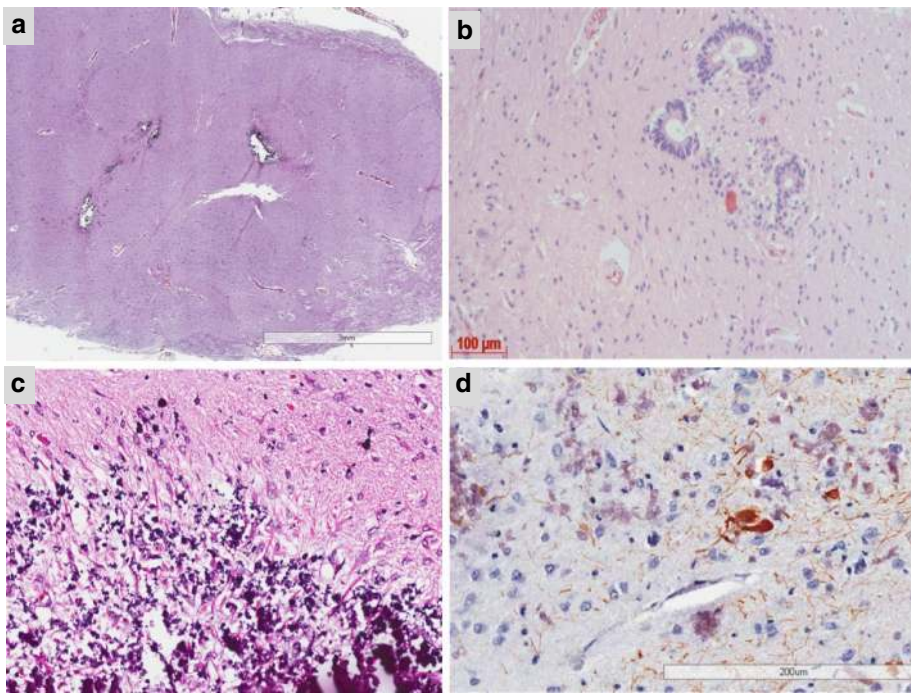

Fig. 5 Case #7—**a** Malformed, distorted midbrain shows calcification and meningeal glioneuronal heterotopia (*right bottom side* of the picture), and is associated with aqueduct stenosis (**b**) characterized by small and displaced branching channels. **c** coarse and filamentous calcification and extensive gliosis over the brainstem, where axons, immunostained with neurofilament (**d**), are directionally disrupted and degenerated, forming axonal spheroids. **a**, **b**, **c** (H&E)

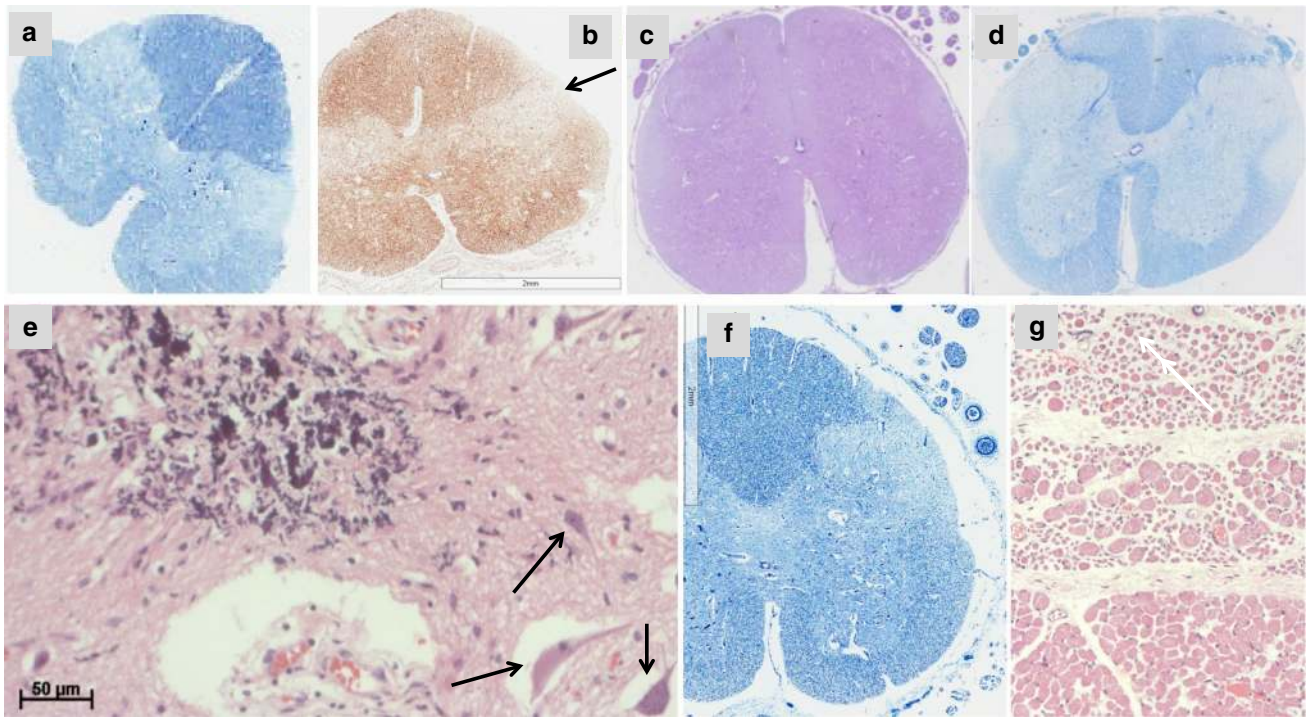

Fig. 6 Sections of abnormally shaped cervical spinal cord from case #7 (**a**, **b**, **f**) due to lack of the lateral cortico-spinal tracts, in addition to thin ventral roots (*bottom right*—**f**), compared to the normal dorsal roots (**f**—*top right*). In **b**, the lack of axons in the lateral cortico-spinal tract is confirmed (*arrow*). The dorsal column is well populated in axons and myelin (**a**, **b**, **f**). For comparison, although not at the same level, a normally shaped lumbar spinal cord (from case #10), with normal lateral cortico-spinal tracts (**c**, **d**), not completely myelinated at this age (**d**). **e** Coarse calcification in the spinal anterior horn (case #2), with few remaining motor nerve cells (*arrows*). **g** Muscle psoas showing many atrophic fibers, which predominate in the fascicle at the top, are intermingled with hypertrophic fibers in the middle, while the fascicle at the bottom is less affected. H&E (**c**, **e**, **g**), LFB (**a**, **d**, **f**), immunostaining with neurofilament (**b**)

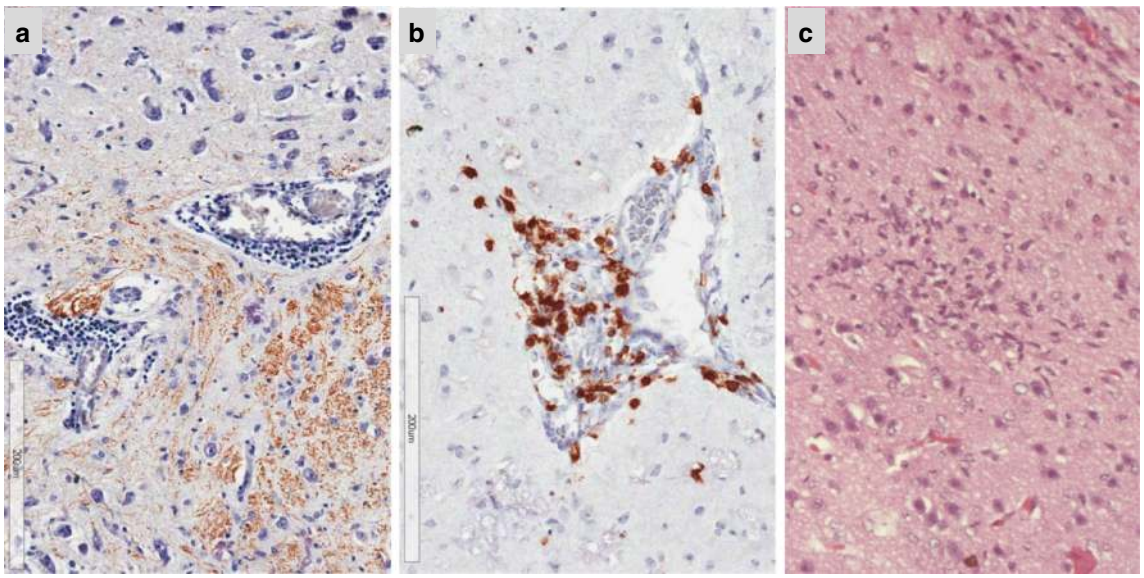

Fig. 7 **a**, **b** Case #3—perivascular parenchymal lymphocytes in the brainstem immunostained with neurofilament, and perivascular parenchymal CD8+ T-lymphocytes (**b**). The microglial nodule of case #9 is illustrated in **c** (H&E)

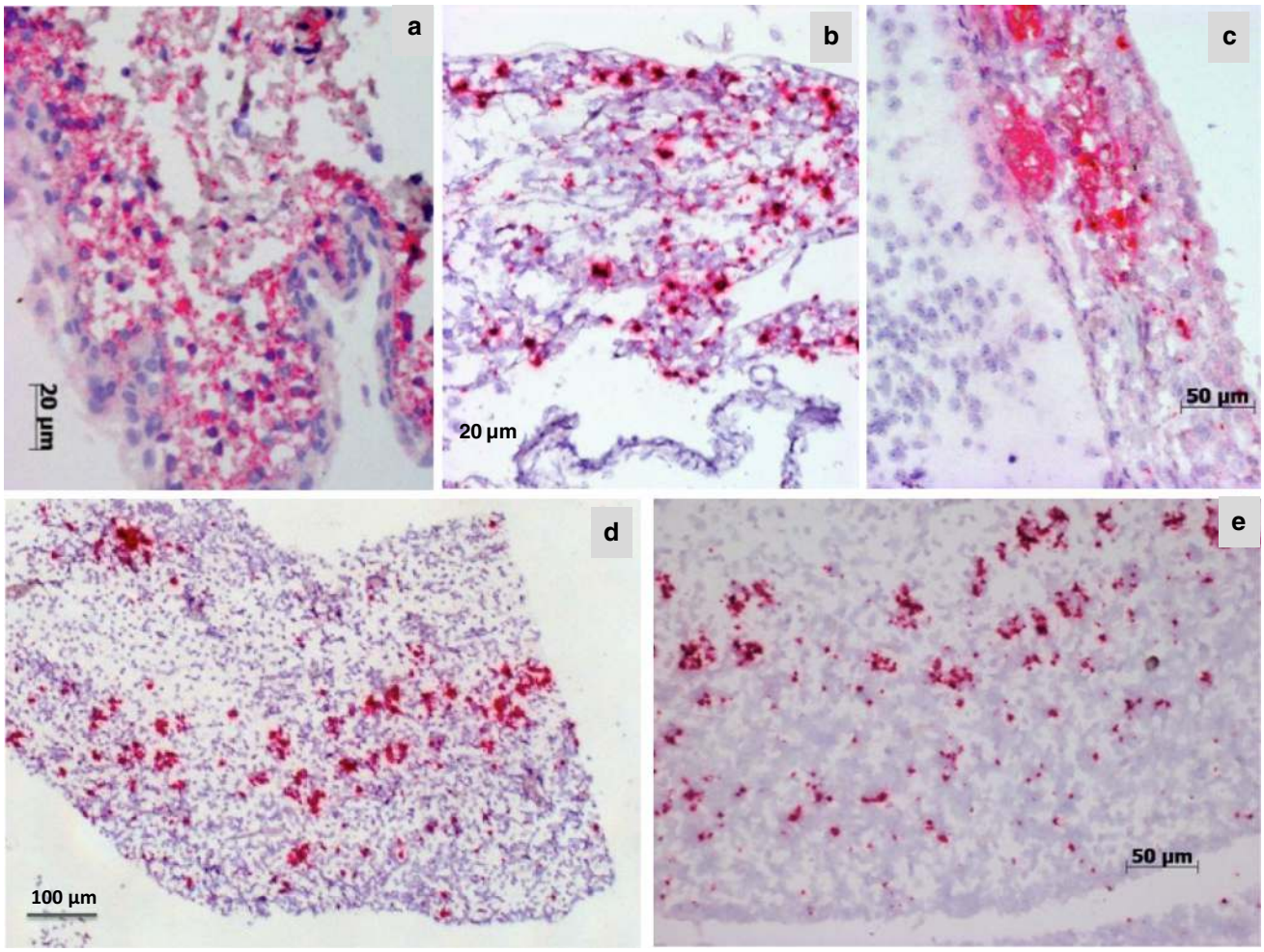

Fig. 8 Positive ISH with Zika probes in the meninges of cases #3, 5, 9 (**a**, **b**, **c**) and in the germinal matrix of case #5 (**d**, **e**)

in several cases and in the germinal matrix and neocortex in one case. It was frequently detected in hepatocytes, collecting tubules of kidney, and red pulp of the spleen, and occasionally in the heart and adrenal glands.

The neuropathological lesions

Overall, the weight of the brain was disproportionately lower than expected for the gestational ages [25]. In our series, lesions were very similar to previously reported cases [12, 14, 29, 32], consisting of almost complete agyria, pachygyria, mild lympho-histiocytic infiltration, reactive astrocytosis, and multifocal dystrophic calcifications, the latter, a reaction to tissue damage, including apoptosis, as observed in some of our cases, corroborating the previous findings of cleaved-caspase-3-positive apoptotic cells in experimental infection [9].

Most of the babies included in our study were delivered at the end of gestation, allowing the pathological process to progress. Overall, they showed a spectrum of lesions of various severities, always destructive/calcified, with consequent hypoplasia and migration disturbances.

We could group the lesions in three well-defined patterns. The first pattern consisted of various degrees of asymmetric ventriculomegaly in which the hemispheres were thin, always with severe brainstem damage, including aqueduct stenosis or distortion and coarse calcification. This pattern was present in five cases (#1, 2, 3, 7, and 9). The second pattern consisted of small brains, mild-to-moderate ventriculomegaly (ex-vacuo), hemispheric calcification, and hypoplastic brainstem, but without destructive lesions/coarse calcification in the midbrain, and the aqueduct was patent or even dilated. This second pattern was present in four cases (#4, 5, 6, and 8). In patterns 1 and 2, ZIKV infection had occurred in the first or beginning of the second trimester of gestation and the cause of death was the severity of the cerebral damage, the first related to the malformations in the brainstem and intracranial hypertension. We believe that the brainstem lesions were responsible for the

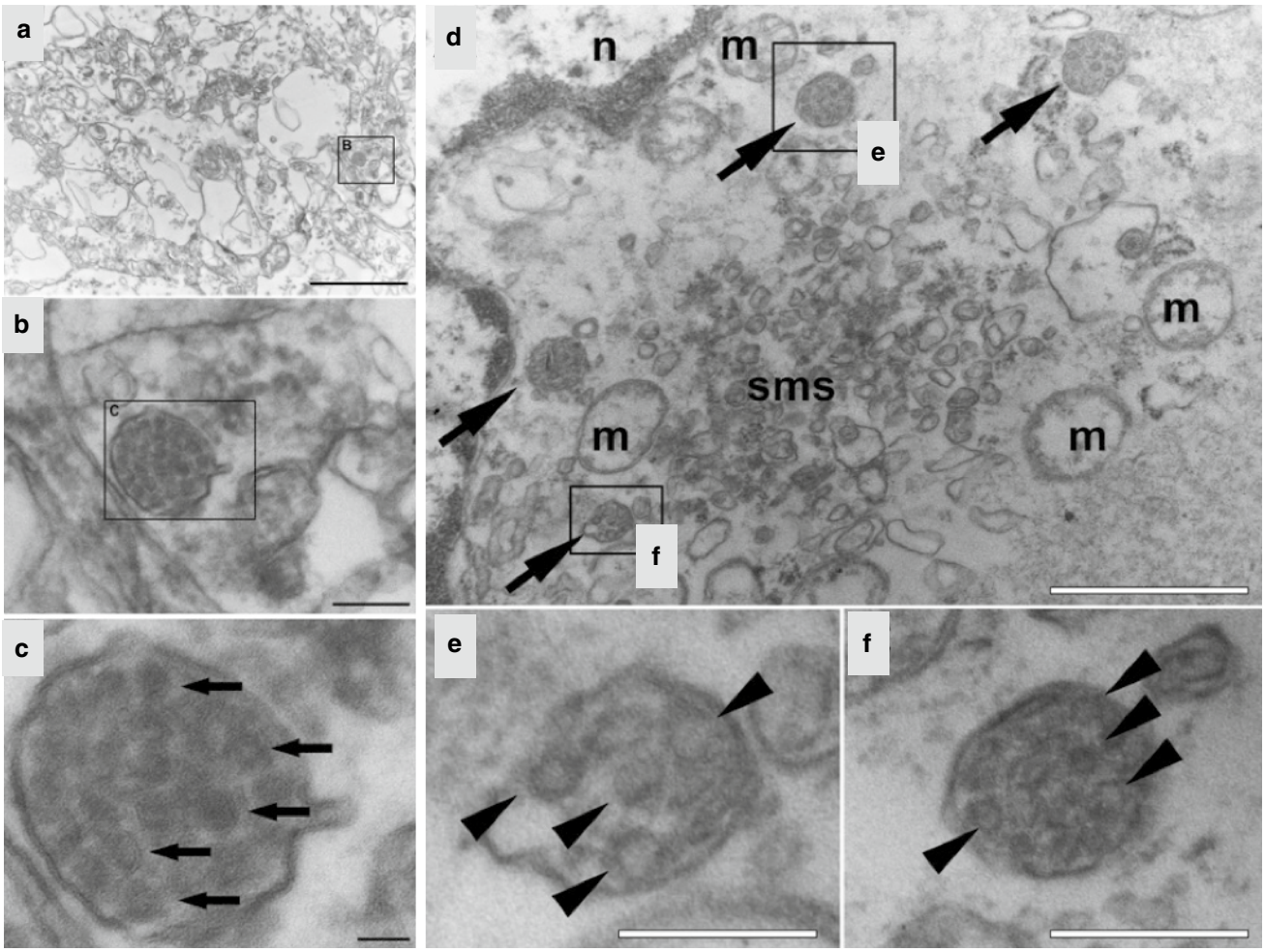

Fig. 9 **a**, **b**, **c** (case #9): Ultrastructure of subpial fragment showing poorly preserved neuropil (**a**). Inset in (**a**) depicts a vesicle containing many viral particles. Higher magnification of inset in (**a**) highlights the presence of virus particles (**b**) and higher magnification of inset in **b** shows vesicle with dense aggregation of viruses (*arrows*) in detail (**c**). **d**, **e**, **f** (Germinal matrix of case #5) (**d**) Low magnification image showing smooth membrane structures (sms) concentrated in the cytoplasm and vesicles containing viral particles (*arrows*), degenerated mitochondria (m), and a nucleus profile (n). Higher magnification of insets (**e** and **f**) shows viral particles indicated by arrowheads. *Scale bars* 2 μm in **a**; 200 nm in **b**; 50 nm in **c**; 1 μm in **d**; 250 nm in **e**; 300 nm in **f**

obstructive hydrocephalus. However, the reason for the destructive brainstem lesions in pattern 1 needs to be further elucidated. The third pattern, a well-developed CNS, had only coarse hemispheric calcification, mild gliosis, and occasional clusters of immature cells in deep white matter. This pattern was seen in patient #10, whose infection occurred in the third trimester with mild damage to CNS, suggesting that the timing of infection during gestation is crucial to the clinical outcome, corroborating the previous report of increasing risk of brain damage in ZIKV infections early during gestation [22]. On the other hand, an ischemic cause to explain the different patterns cannot be ruled out, as discussed below.

Primary destruction with calcification is the common process to all cases.

The hypoplasia of various structures may be a result of distinct but related phenomena (a) primary infection of neuroglial progenitor cells resulting in dysgenetic migration; (b) disturbance (through transient ischemia or inflammation) of cell migration; and (c) destruction of sites leading to subsequent atrophy or hypotrophy (e.g., cortico-spinal tracts). Some of these changes were also described in isolated reports, particularly in a more detailed neuropathological description [44] of the first reported fetus [32].

Striking abnormalities including lack of lateral cortico-spinal tract were also seen in the spinal cords. The motor nerve cell loss, gliosis and calcification, could explain the intrauterine akinesia and consequent arthrogryposis. Curiously, in patient #2, whose arthrogryposis

affected the upper limbs only, the motor nerve cell loss was limited to the cervical spinal cord, suggesting that arthrogryposis is due to lower motor nerve cell loss, rather than the lack of upper motor nerve fibres related to the severe cortical damage. In fact, samples of skeletal muscle from these patients, except from the lower limb of patient #2, showed neurogenic atrophy. Of note, the sensory nervous system (represented by the DRG in this series) and the dorsal roots and column of the spinal cords were normal. One can speculate that DRG neurons derive from the neural crest, instead of the neural tube (escaping neuronal viral tropism such as in poliomyelitis and WNV encephalitis [27]), and/or that their maturation occurs later than that of the motor neurons [45], when the infection was possibly not active.

Imaging features

Fetal microcephaly or other malformations involving the nervous system were demonstrated with ultrasonography, as in several other series [5, 11, 32, 34, 37, 41], one of them [41] included three patients from our series. They consisted of parenchymal calcifications, particularly in gray–white matter junction, the basal ganglia and/or thalamus, callosal dysgenesis, polymicrogyria, hypoplasia of the cerebellar vermis and cerebellum, ventriculomegaly, and also extensive joint alterations in legs and arms. When microcephaly was severe, the skull had a collapsed appearance with overlapped sutures and redundant and folded skin in the occipital region, indicating that the head and skin continued to grow, while the size of the brain regressed. However, when the ventricles grew, the circumference of the head was normal or even increased [41], justifying the recommendation to avoid the term microcephaly to define congenital Zika infection [31].

Direct CNS viral infection

It is well recognized that transplacental transmission of viruses even with subclinical maternal infection can lead to severe congenital abnormalities. It is also already known that ZIKV crosses the fetal-placental barrier. ZIKV has been isolated from the brains and CSF of neonates born with microcephaly and identified with immunohistochemistry in the placenta of mothers who had symptoms of ZIKV infection during their pregnancies [12, 29]. With ISH, we did not detect virus in the placentas, probably due to the time passed between the date of infection and the birth.

The fact that, in our case series, most mothers had symptoms in the first trimester of gestation, and the premature baby (patient #5), with the shortest interval between infection and birth (22 weeks), had the smallest brain, and virus in the cerebral germinal matrix, suggest that infection of fetal neural progenitors could induce cell death and interfere with proliferation and neuronal migration during a time of rapid brain development, as demonstrated in our cases and in some experimental models [9, 17, 19, 46]. The fact that the virus was not detected directly in the brain tissue in other cases could be explained by the birth around the 40th week of gestation when infected cells might have already disappeared or failure of virus to penetrate a more mature blood–brain barrier. However, in leptomeningeal vessels, the virus was still present, particularly in case #9, whose mother reported symptoms at the beginning of the 2nd trimester, but the viral load in amniotic fluid and tissues (including brain) was very high and the brain was severely damaged. As previously suggested [31], this was probably because the mother's symptoms of Zika (itching and rash) were mistakenly diagnosed as allergic reaction and treated with corticosteroids, which may have impaired immunity, allowing viral replication and increased brain damage. In fact, prolonged viremia has been reported contributing to fetal brain abnormalities [14].

The Brazilian strain of ZIKV interferes with the cellular machinery controlling neural proliferation and alters the expression of more than 500 genes responsible for guiding the formation of the brain. The molecular pathways associated with ZIKV infection reveal activation of DNA repair machinery, cell cycle arrest, and down regulation of genes driving neural specialization [18]. A significant increase in mitosis abnormalities and apoptotic cell death of neural progenitors after cell division were also described [43]. It has been put forward the idea that ZIKV crosses the placenta barrier and reaches the developing brain by blood born dissemination or through the CSF [33]. The presence of virus in the leptomeninges in our cases may support the hypothesis that to enter the brain parenchyma, ZIKV must pass the glia limitans, an array of neuroglial cells that form borders that separate neural from nonneural tissue along perivascular spaces, meninges, and tissue lesions in the CNS. In fact, the frequent over-migration of the nervous tissue into the subarachnoid space, also more marked in case #9, with the cobblestone appearance of the cortical surface, may be due to more severe damage of the glia limitans. ZIKV may, therefore, interact with neuroglial cells that include the radial glia, a possible stem cell target for ZIKV. The receptor AXL, identified in the human radial glia, brain microcapillaries, microglia, and in cortical astrocytes in the developing human brain, is a candidate receptor for ZIKV in neuronal stem cells [23, 33]; however, other key viral entry receptors should also be considered [48].

Differential diagnosis with other causes of congenital infection

Microcephaly has many causes, most commonly infections (TORCHS, HIV), but also teratogens (maternal exposure to heavy metals, alcohol, and radiation), genetic abnormalities and syndromes, and growth restriction [16, 27, 47]. In some of the infections, the agent, intra-nuclear inclusions, or the parasite itself is identified, which was not the case in our series. In some of the infections, the brain calcifications were mainly periventricular, also not observed in our cases, and microglial nodules were frequent, but only one was seen in this series. In toxoplasmosis, collapsed hydrocephalic brains (and multifocal cortical calcification) may occasionally be observed [16]. The predominance of nerve cell degeneration and calcification in the thalamus and brainstem, in addition to motor nerve cell loss in the spinal cord and microphthalmia, are reminiscent of the histological findings of Japanese encephalitis virus infection, another flavivirus member [27], although not related to congenital infection in humans. On the other hand, congenital infection has been reported in dengue [3] and WNV encephalitis [1], the latter with ocular and neurologic morbidity (CNS malformation in a newborn).

Secondary ischemic process

Due to the topography and morphology of some of the CNS lesions, and the fact that in none of the hydrocephalic brains, the virus was identified in the cerebral parenchyma, we cannot discard the hypothesis of an ischemic process in the pathogenesis of the destructive lesions. Radiologists have reported that intraparenchymal calcifications associated with Zika are more severe than those typically seen in TORCHS infections. Moreover, the gray–white matter interface is not a classical topography for calcifications in other congenital infections [41]. Although in brains with very little cortical mantle, we could not evaluate the topography of calcification, in those with thicker hemispheres and in the patient born with a well-developed brain (#10), the calcification was in the white matter or gray–white matter interface. On the other hand, infection of the meninges would be expected to mediate direct or indirect vascular damage and subsequent destruction of dependent CNS structures. We did not interpret as hydranencephaly the extreme thinning of the cerebral mantle, which could raise the possibility that vascular compromise only could be playing a role in the pathogenesis of the lesions, because this group of cases had always marked midbrain calcification, distortion, and aqueduct stenosis, suggesting that the primary pathological process was destructive, affecting both posterior fossa structures and the cerebral hemispheres, and that the latter were further damaged by the increased intracranial pressure. An argument in favor of an ischemic process is the histological evidence of villitis, maternal vascular underperfusion, and hypoxia, including chorangiosis. In fact, placental insufficiency characterized by abnormal arterial flow in umbilical cord and brain has been previously reported in association with congenital ZIKV infection [5]. In at least two cases, there was also evidence of maternal hypertension, which could have contributed to fetal ischemic distress, including the subependymal hemorrhage and cerebellar necrosis present in case #5, the same with myocardial infarct; of note, the only with ZIKV in the germinal matrix.

Systemic effects of infection

Although significant morphologic changes were limited to the CNS and systemic organs had mild changes, it is worth mentioning that mild hepatitis with presence of the virus, detected also in renal tubules and the red pulp of the spleen, indicate hematogenous circulation as has been reported in WNV infection [27].

Probably, other factors related to immunity, maternal nutrition, and individual factors interfering with placental and fetal development might contribute to the ZIKV-associated neuropathologic sequelae and should be further investigated to explain the different spectrum of the lesions.

Conclusions

We characterized in congenital ZIKV infection the neuropathological lesions according to topography and severity. Spectrum of neuropathological changes was related to the gestational time of infection. Localization of ZIKV in the CNS and systemic organs suggests the pathogenesis of the disease process. We hypothesize that in early gestational age, CNS lesions can result from direct infection of neuroglial elements, while later stage infections mediate CNS destruction through an ischemic consequence of leptomeningeal infection.

Acknowledgements We thank Débora Silva, Diego Santos, and Luciana Bitana for technical assistance in histological and immunohistochemical preparations, and Centro Nacional de Biologia Estrutural e Bioimagem (CENABIO) for technical assistance in transmission electron microscopy. These studies received partial support from the National Institute of Health (NIH) IH NIAID grant U01 AI 111598 (C.A.W.) and from Conselho Nacional de Desenvolvimento Científico e Tecnológico [CNPq] and Fundação de Amparo a Pesquisa do Rio de Janeiro [FAPERJ] (A.T).

Author contribution LC, CAW, ASOM, RSA, and AT designed the study; ASOM, MEM, AGMB, MMRA, FM, TAF, JRLM, and JIBFL managed the patients; FT-M and PSO-S conducted the

imaging analysis; GSA, MBA, RMB, and RD did the laboratory studies; AGMB, EA-P, VSL, HNM, CVAM, DCAD, ACGC, and ONU performed the autopsies; LC, AHSC, and EA-P conducted the neuropathological and histopathological investigations. CAW was responsible for the ISH studies; RFMC and SR conducted the ultrastructural studies; LC, CAW, ASOM, FT-M, PSO-S, EA-P, SR, MBA, RMB, RD, RSA, and AT analyzed the results. LC, CAW, FT-M, RSA, and AT wrote and edited the initial drafts. All authors reviewed the final manuscript.

Compliance with ethical standards

Conflict of interest The authors declare that they have no conflict of interest.

Informed consent Informed consent was obtained from all parents of participants included in the study.

References

1. Alpert SG, Fergerson J, Noël LP (2003) Intrauterine West Nile virus: ocular and systemic findings. Am J Ophthalmol 136:733–735. doi:10.1016/S0002-9394(03)00452-5
2. Araujo AQ, Silva MT, Araujo AP (2016) Zika virus-associated neurological disorders: a review. Brain 139:2122–2130. doi:10.1093/brain/aww158
3. Basurko C, Carles G, Youssef M, Guindi WEL (2009) Maternal and fetal consequences of dengue fever during pregnancy. Eur J Obstet Gynecol Reprod Biol 147:29–32. doi:10.1016/j.ejogrb.2009.06.028
4. Besnard M, Eyrolle-Guignot D, Guillemette-Artur P, Lastère S, Bost-Bezeaud F, Marcelis L et al (2016) Congenital cerebral malformations and dysfunction in fetuses and newborns following the 2013–2014 Zika virus epidemic in French Polynesia. Euro Surveill. doi:10.2807/1560-7917.ES.2016.21.13.30181
5. Brasil P, Pereira JP Jr, Raja Gabaglia C, Damasceno L, Wakimoto M, Ribeiro Nogueira RM et al (2016) Zika virus infection in pregnant women in Rio de Janeiro. N Engl J Med 375:2321–2334. doi:10.1056/NEJMoa1602412
6. Brien JD, Uhrlaub JL, Hirsch A, Wiley CA, Nikolich-Zugich J (2009) Key role of T cell defects in age-related vulnerability to West Nile virus. J Exp Med 206:2735–2745. doi:10.1084/jem.20090222
7. Campos GS, Bandeira AC, Sardi SI (2015) Zika virus outbreak, Bahia, Brazil. Emerg Infect Dis 21:1885–1886. doi:10.3201/eid2110.150847
8. Carteaux G, Maquart M, Bedet A, Contou D, Brugieres P, Fourati S et al (2016) Zika virus associated with meningoencephalitis. N Engl J Med 374:1595–1596. doi:10.1056/NEJMc1602964
9. Cugola FR, Fernandes IR, Russo FB, Freitas BC, Dias JLM, Guimarães KP et al (2016) The Brazilian Zika virus strain causes birth defects in experimental models. Nature 534:267–271. doi:10.1038/nature18296
10. Dasti JI (2016) Zika virus infections: an overview of current scenario. Asian Pac J Trop Med 9:621–625. doi:10.1016/j.apjtm.2016.05.010
11. de Fatima Vasco Aragao M, van der Linden V, Brainer-Lima AM, Coeli RR, Rocha MA, Sobral da Silva P et al (2016) Clinical features and neuroimaging (CT and MRI) findings in presumed Zika virus related congenital infection and microcephaly: retrospective case series study. BMJ 353:i1901. doi:10.1136/bmj.i1901
12. de Noronha L, Zanluca C, Azevedo MLV, Luz KG, dos Santos CND (2016) Zika virus damages the human placental barrier and presents marked fetal neurotropism. Mem Inst Oswaldo Cruz 111:287–293. doi:10.1590/0074-02760160085
13. Dick GWA (1952) Zika virus (I). Isolations and serological specificity. Trans R Soc Trop Med Hyg 46:509–520. doi:10.1016/0035-9203(52)90042-4
14. Driggers RW, Ho C-Y, Korhonen EM, Kuivanen S, Jääskeläinen AJ, Smura T et al (2016) Zika virus infection with prolonged maternal viremia and fetal brain abnormalities. N Engl J Med 374:2142–2151. doi:10.1056/NEJMoa1601824
15. Duffy MR, Chen T-H, Hancock WT, Powers AM, Kool JL, Lanciotti RS et al (2009) Zika virus outbreak on Yap Island, Federated States of Micronesia. N Engl J Med 360:2536–2543. doi:10.1056/NEJMoa0805715
16. Ellison D, Love S, Chimelli LMC, Harding B, Lowe JS, Vinters HV et al (2012) Neuropathology: a reference text of CNS pathology. Elsevier, Amsterdam
17. Garcez PP, Loiola EC, Madeiro da Costa R, Higa LM, Trindade P, Delvecchio R et al (2016) Zika virus impairs growth in human neurospheres and brain organoids. Science 352:816–818. doi:10.1126/science.aaf6116
18. Garcez PP, Nascimento JM, Mota de Vasconcelos J, Madeiro da Costa R, Delvecchio R, Trindade P et al (2016) Zika virus disrupts molecular fingerprinting of human neurospheres. Sci Rep. 7:40780. doi:10.1038/srep40780
19. Hanners NW, Eitson JL, Usui N, Richardson RB, Wexler EM, Konopka G et al (2016) Western Zika virus in human fetal neural progenitors persists long term with partial cytopathic and limited immunogenic effects. Cell Rep 15:2315–2322. doi:10.1016/j.celrep.2016.05.075
20. Hazin AN, Poretti A, Di Cavalcanti Souza Cruz D, Tenorio M, van der Linden A, Pena LJ, Brito C et al (2016) Computed tomographic findings in microcephaly associated with Zika virus. N Engl J Med 374:2193–2195. doi:10.1056/NEJMc1603617
21. Ioos S, Mallet HP, Leparc Goffart I, Gauthier V, Cardoso T, Herida M (2014) Current Zika virus epidemiology and recent epidemics. Med Mal Infect 44:302–307. doi:10.1016/j.medmal.2014.04.008
22. Johansson MA, Mier-y-Teran-Romero L, Reefhuis J, Gilboa SM, Hills SL (2016) Zika and the risk of microcephaly. N Engl J Med 375:1–4. doi:10.1056/NEJMp1605367
23. Klase ZA, Khakhina S, Schneider ADB, Callahan MV, Glasspool-Malone J, Malone R (2016) Zika fetal neuropathogenesis: etiology of a viral syndrome. PLoS Negl Trop Dis 10:1–32. doi:10.1371/journal.pntd.0004877
24. Lanciotti RS, Kosoy OL, Laven JJ, Velez JO, Lambert AJ, Johnson AJ et al (2008) Genetic and serologic properties of Zika virus associated with an epidemic, Yap State, Micronesia, 2007. Emerg Infect Dis 14:1232–1239. doi:10.3201/eid1408.080287
25. Larroche J-C (1977) Developmental pathology of the neonate. Excerpta Medica, Amsterdam, pp 1–21
26. Likos A, Griffin I, Bingham AM, Stanek D, Fischer M, White S et al (2016) Local mosquito-borne transmission of Zika virus–Miami-Dade and Broward Counties, Florida, June–August 2016. MMWR Morb Mortal Wkly Rep 65:1032–1038. doi:10.15585/mmwr.mm6538e1
27. Love S, Wiley CA, Lucas S (2015) Viral infections. In: Love S, Perry A, Ironside J, Budka H (eds) Greenfield's Neuropathology, 9th edn. CRC Press, London, pp 1087–1191
28. Malone RW, Homan J, Callahan MV, Glasspool-Malone J, Damodaran L et al (2016) Zika virus: medical countermeasure development challenges. PLoS Negl Trop Dis 10:e0004530. doi:10.1371/journal.pntd.0004530

29. Martines RB, Bhatnagar J, de Oliveira Ramos AM, Davi HPF, Iglezias SDA, Kanamura CT et al (2016) Pathology of congenital Zika syndrome in Brazil: a case series. Lancet 388:898–904. doi:10.1016/S0140-6736(16)30883-2
30. Mécharles S, Herrmann C, Poullain P, Tran T, Deschamps N, Mathon G et al (2016) Case report acute myelitis due to Zika virus infection. Lancet 8:6736. doi:10.1136/bcr-2012-007094.4
31. Melo AS, Aguiar RS, Amorim MMR, Arruda MB, de Melo FO, Ribeiro STC et al (2016) Congenital Zika virus infection: Beyond neonatal microcephaly. JAMA Neurol 73:1407–1416. doi:10.1001/jamaneurol.2016.3720
32. Mlakar J, Korva M, Tul N, Popović M, Poljšak-Prijatelj M, Mraz J et al (2016) Zika virus associated with microcephaly. N Engl J Med 374:951–958. doi:10.1056/NEJMoa1600651
33. Nowakowski TJ, Pollen AA, Di Lullo E, Sandoval-Espinosa C, Bershteyn M, Kriegstein AR (2016) Expression analysis highlights AXL as a candidate zika virus entry receptor in neural stem cells. Cell Stem Cell 18:591–596. doi:10.1016/j.stem.2016.03.012
34. Oliveira Melo AS, Malinger G, Ximenes R, Szejnfeld PO, Alves Sampaio S, Bispo De Filippis AM (2016) Zika virus intrauterine infection causes fetal brain abnormality and microcephaly: tip of the iceberg? Ultrasound Obstet Gynecol 47:6–7. doi:10.1002/uog.15831
35. Ramos da Silva S, Gao SJ (2016) Zika virus: an update on epidemiology, pathology, molecular biology, and animal model. J Med Virol 88:1291–1296. doi:10.1002/jmv.24563
36. Sarno M, Sacramento GA, Khouri R, do Rosário MS, Costa F, Archanjo G et al (2016) Zika virus infection and stillbirths: a case of hydrops fetalis, hydranencephaly and fetal demise. PLoS Negl Trop Dis 10:e0004517. doi:10.1371/journal.pntd.0004517
37. Schuler-Faccini L, Ribeiro EM, Feitosa IML, Horovitz DDG, Cavalcanti DP, Pessoa A et al (2016) Possible association between zika virus infection and microcephaly—Brazil, 2015. MMWR Morb Mortal Wkly Rep 65:59–62. doi:10.15585/mmwr.mm6503e2
38. Schwartz DA (2016) Autopsy and postmortem studies are concordant: pathology of Zika virus infection is neurotropic in fetuses and infants with microcephaly following transplacental transmission. Arch Pathol Lab Med 141(1):68–72. doi:10.5858/arpa.2016-0343-OA
39. Slavov SN, Otaguiri KK, Kashima S, Covas DT (2016) Overview of Zika virus (ZIKV) infection in regards to the Brazilian epidemic. Brazilian J Med Biol Res 49:e5420. doi:10.1590/1414-431X20165420
40. Snijders RJ, Nicolaides KH (1994) Fetal biometry at 14–40 weeks' gestation. Ultrasound Obstet Gynecol 4:34–48. doi:10.1177/875647939401000434
41. Soares de Oliveira-Szejnfeld P, Levine D, de O Melo AS, Amorim MMR, Batista AGM, Chimelli L et al (2016) Congenital brain abnormalities and zika virus: what the radiologist can expect to see prenatally and postnatally. Radiology 281:203–218. doi:10.1148/radiol.2016161584
42. Solomon IH, Milner DA, Folkerth RD (2016) Neuropathology of Zika virus infection. J Neuroinfect Dis 7(2):220
43. Souza BS, Sampaio GL, Pereira CS, Campos GS, Sardi SI, Freitas LAR et al (2016) Zika virus infection induces mitosis abnormalities and apoptotic cell death of human neural progenitor cells. Sci Rep 6:39775. doi:10.1038/srep39775
44. Štrafela P, Vizjak A, Mraz J, Mlakar J, Pižem J, Tul N et al (2016) Zika virus-associated micrencephaly: a thorough description of neuropathologic findings in the fetal central nervous system. Arch Pathol Lab Med 141:73–81. doi:10.5858/arpa.2016-0341-SA
45. Tadros MA, Lim R, Hughes DI, Brichta AM, Callister RJ (2015) Electrical maturation of spinal neurons in the human fetus: comparison of ventral and dorsal horn. J Neurophysiol 114:2661–2671. doi:10.1152/jn.00682.2015
46. Tang H, Hammack C, Ogden SC, Wen Z, Qian X, Li Y et al (2016) Zika virus infects human cortical neural progenitors and attenuates their growth brief report Zika virus infects human cortical neural progenitors and attenuates their growth. Cell Stem Cell 18:587–590. doi:10.1016/j.stem.2016.02.016
47. Teissier N, Fallet-Bianco C, Delezoide A-L, Laquerrière A, Marcorelles P, Khung-Savatovsky S et al (2014) Cytomegalo virus-induced brain malformations in fetuses. J Neuropathol Exp Neurol 73:143–158. doi:10.1097/NEN.0000000000000038
48. Wells MF, Salick MR, Wiskow O, Ho DJ, Worringer KA, Ihry RJ et al (2016) Genetic ablation of AXL does not protect human neural progenitor cells and cerebral organoids from Zika virus infection. Cell Stem Cell 19:703–708. doi:10.1016/j.stem.2016.11.011
49. Zanluca C, Melo VC, Mosimann AL, dos Santos GI, dos Santos CN, Luz K (2015) First report of autochthonous transmission of Zika virus in Brazil. Mem Inst Oswaldo Cruz 110:569–572. doi:10.1590/0074-02760150192